RESEARCH ARTICLE

Analysis of the degradation of single–crystalline silicon modules after 21 years of operation

M. Piliougine PhD[1] | A. Oukaja MSc[2] | P. Sánchez-Friera PhD[3] | G. Petrone PhD[1] | F.J. Sánchez-Pacheco PhD[4] | G. Spagnuolo PhD[1] | M. Sidrach-de-Cardona PhD[5]

[1]Dipartimento di Ingegneria dell'Informazione ed Elettrica e Matematica Applicata/DIEM – University of Salerno. Via Giovanni Paolo II 132. 84084 Fisciano (SA), Italy

[2]Universidad Internacional de Andalucía. 29007 Málaga, Spain

[3]Solkeys. 33204 Gijón,Spain.

[4]Departamento de Tecnología Electrónica – Universidad de Málaga. 29071 Málaga, Spain

[5]Departamento de Física Aplicada II – Universidad de Málaga. 29071 Málaga, Spain

Correspondence
M. Piliougine PhD.
Email: mpiliouginerocha@unisa.it

Funding information
Ministerio de Ciencia, Innovación y Universidades [RTI2018–095097–B–I0]; Ministero dell'Istruzione, dell'Università e della Ricerca [2017WA5ZT3003]; Università degli Studi di Salerno (FARB funds)

In this paper the results of the analysis of the degradation of a set of single–crystalline silicon modules after 21 years are presented. The comparison of the main electrical parameters and the series and of the shunt resistances measured in 1996 and 2017 is performed, so that the annual degradation rate is evaluated. In addition, a detailed analysis of the parameter uncertainties has been performed in order to determine its impact on the results. A visual inspection of the modules has also been carried out in order to show the correlation with the variation of the electrical performance. Finally, the temperature coefficients of the degraded modules have been estimated and compared with the nominal ones. The results shown in the paper reveal that the mean annual degradation rate in terms of power is close to 0.9%.

KEYWORDS
I–V curve correction, outdoor measurement, photovoltaic degradation, temperature coefficient, uncertainty analysis, visual defect

1 | INTRODUCTION

The output power of a photovoltaic (PV) device decreases throughout time. This decrease is due to its exposure to solar radiation as well as to other external conditions. The degradation ratio, which is defined as the annual percentage loss of output power, is a key factor to determine the long–term production of a PV plant. In–depth knowledge of the annual degradation rate is required to have accurate estimations of the energy generation of a PV plant along its lifetime. A full understanding of the mechanisms involved in degradation requires on-field measurements of modules exposed for long periods of time under real operating conditions. Alternatively, in-lab accelerated ageing tests can contribute to the analysis of these mechanisms and the rapid identification of typical failures [1]. To gain insight into the degradation mechanisms, it is worth to quantify separately the percentage of decay associated to each of the electrical parameters, such as short–circuit current, open–circuit voltage or fill factor, since they do not affect the electrical performance of the photovoltaic system in the same way. It should be taken into account that the individual degradation of a PV module can significantly influence the performance of a complete string. In addition, not all the modules in the same installation decrease their performances at exactly the same rate. Given a set of modules exposed to long–term outdoor conditions, the individual degradation of the main electrical parameters as well as the increase in their dispersion have to be considered. As each module tends to degrade in a different way, the behavior of the modules will be more and more different as time goes by, thus affecting negatively the global performance of the plant.

According to Köntges et al. [2], a module defect is an irreversible damage that causes either a degradation in terms of power or a security risk. These defects can be classified in different categories as a function of several criteria, such as the moment in which they appear. Thus there might be initial defects, which arise during the installation or in the first two years of operation, middle–age defects, appearing after some years of exposure, and wear defects, occurring at the end of the module's useful life. The modules considered in this paper have been in operation for 21 years, thus their defects fall into the second/third of the above groups. Degradation mechanisms and rates depend on the climatic conditions of the region, especially on factors such as solar irradiance, temperature, humidity and air salinity, and also on the operating conditions of the PV system. Some of the defects can be visualized as physical anomalies that can be detected by a simple visual inspection. Examples of common visible anomalies are: discoloration, which is related to the degradation of the physical properties of encapsulating materials; detachment of the back layer and junction boxes; cracks in the glass and solar cells; and burned cells due to hot–spots. Other signs related to degradation are not easily observed by visual inspection, but they can nevertheless have a large impact in the output power. They are, for instance, related to failures in electrical connections, shunts formation, microcracks in the cells, p–n junction degradation, and defective bypass diodes, among others.

There are several studies dealing with the analysis of the power degradation of modules based on different PV technologies available in the literature. Table 1 summarizes annual degradation rates for single–crystalline silicon (sc–Si) modules, together with the total power loss and the length of the exposure period under study. It is evident that the annual degradation of the maximum power ranges between 0.8% and 1.0%, with some exceptions above and below.

The values of the main electrical parameters of different modules after 20 years of exposure to external conditions are examined in Pozza and Sample [3]. A correlation of the obtained results with visual inspection and other complementary techniques is performed therein. The browning of the EVA layer is recognized as the most frequent damage and it is primarily responsible for the short–circuit current reduction. Other problems, such as the corrosion of the metal bus–bars, are also present and affect mainly the open–circuit voltage.

Reference	Manufacturer/model	Power loss	Years	Annual rate
Cereghetti et al. [4]	Isofotón I–110	0.8%	1	≈0.8%
Cereghetti et al. [4]	Atersa A–60	0.8%	1	≈0.8%
Osterwald et al. [5]	BP Solar BP–585F	2.1%	7	≈0.3%
Osterwald et al. [5]	BP Solar BP–270F	2.56%	8	≈0.32%
Osterwald et al. [5]	Siemens PC–4–JF	4.8%	9.5	≈0.51%
Sánchez–Friera et al. [6]	Isofotón I–53	11.5%	12	≈0.96%
Ishii et al. [7]	PV5a (not specified)	2.4%	3	≈0.8%
Ishii et al. [7]	PV5b (not specified)	1.93%	3	≈0.64%
Ishii et al. [7]	PV6 (not specified)	2.77%	3	≈0.92%
Charrouf et al. [8]	Isofotón I–75	17.4%	10	≈1.74%
Lorenzo et al. [9]	Isofotón (60 cells)	9%	17	≈0.54%

TABLE 1 Summary of different studies of degradation for sc–Si modules.

In Chattopadhyay et al. [10], a study of the visual defects of several modules subjected to different weather conditions is shown. Most of the sc–Si modules have a period of operation between 10 and 30 years. Corrosion problems appear to be typical in climatic conditions with high humidity and temperature. The loss of transparency of the glass and of the encapsulating material in front of the cell have a strong effect on the short–circuit current. Likewise, the corrosion of the metal tapes between the bus–bars cells increases the series resistance.

In Kaplani [11], several crystalline silicon modules affected by long–term defects are analyzed, e.g. cell cracks, frontal delamination, browning of the EVA layer, corrosion of the metal tapes and changes in the anti–reflective layer of the cells. This analysis is supported by thermography, electroluminescence, fluorescence with ultraviolet radiation and I–V curve measurements.

The degradation of the PV modules under analysis in this paper had already been studied in a previous article. Sánchez–Friera et al. [6] present an analysis of the system after 12 years of operation, showing some evident defects related to the variation of the electrical parameters. The main defects were permanent soiling, i.e. blurred or dark area at the bottom edge of the modules, oxidation of the front metallization finger and the anti–reflexive layer, and frontal delamination. They are the main contributors to the registered 9.2% decrease in the short–circuit current during these initial 12 years. In terms of maximum power, the total losses have been 11.5% in comparison with the measurements 12 years before, so that the average power decreased by 0.96% per year.

In the present research, the analysis of the sc–Si PV module degradation in the above study is further extended, so that it now covers a 21 year exposure period, from 1996 to 2017. The comparative analysis is based on the main electrical parameters, on the values of the series resistance R_s, and of the shunt resistance R_{sh}, that are identified from the measured I–V curves. The results of visual inspection are shown and the different defects have been identified and classified, so that a relationship between the visual defects and the decrease of the main electrical parameters is determined. Finally, the temperature coefficients of the degraded PV modules have been estimated and compared to the nominal ones provided by the manufacturer.

This work is organized as follows: in Section 2 the procedures used to extract the information about the PV modules health state at the beginning and at the end of the period under analysis are explained. The results of the comparative analysis are presented in Section 3. The main conclusions of the study are summarized in Section 4.

2 | METHODOLOGY

The PV modules under study were manufactured by *Isofotón S.A.* and are of the model I–53, whose main features at standard test conditions (STC) are summarized in Table 2. They are composed of 36 pseudosquare sc–Si cells with side ≈ 103 mm, all connected in series [12]. The values of the series resistance (R_s) and the temperature coefficients (α, β, γ and κ) were provided directly by the manufacturer through an internal communication.

N_s	P_{max}	I_{SC}	V_{OC}	I_{Pmax}	V_{Pmax}	R_s	α	β	γ	κ
	(W)	(A)	(V)	(A)	(V)	(mΩ)	(mA/°C)	(mV/°C)	(mW/°C)	(mΩ/°C)
36	53	3.27	21.6	3.05	17.4	288	+1.29	−80	−256	+0.86

α, β, γ, and κ are the temperature coefficients of I_{SC}, V_{OC}, P_{max}, and R_s respectively.

TABLE 2 Nominal parameters of the Isofotón I–53 at STC.

The modules used in this work have been selected from an installation located on the terrace of the Laboratory of Photovoltaic Systems of the University of Málaga. This generator had initially 42 PV modules, but a few years later it was extended to 54 units. It has been operating under real conditions for 21 years, with several series/parallel configurations as the system was used to test different grid tied inverters. The main characteristics of the system are shown in Table 3.

Latitude	Longitude	Elevation	Inclination	Azimuth	Initial year	Intermediate year	Final year
36.715° N	4.478° W	50 m	45°	10° W	1996	2008	2017

TABLE 3 Information about the location of the installation.

In addition to the measurements from the 1996 and from 2017, the PV modules under study were also characterized in the summer of 2008, as reported in [6], so that it is possible to distinguish between two different exposure periods. The meteorological conditions given in both periods and in the total exposure time have been provided by AEMET [13] and they are summarized in Table 4.

	Mean daily max. temp. (°C)	Mean daily min. temp. (°C)	Mean annual rain (L/m^2)	Mean wind speed (m/s)	Mean daily sun hours (h)
First period (from 1996 to 2008)	23.6	14.3	561	2.5	8.1
Second period (from 2008 to 2017)	24.2	15.2	516	2.3	8.3
Total period (from 1996 to 2017)	23.9	14.7	546	2.4	8.2

TABLE 4 Meteorological conditions in the different exposure periods

2.1 | Characterization of the PV modules

All the *I*–*V* curves were **measured outdoors** at around solar noon and under perfect clear–sky conditions in all three measurement campaigns, conducted in the summers of 1996, 2008 and 2017. Since in our emplacement, the typical values of the normal irradiance G at noon in these conditions are significantly greater than 1 000 W/m^2, we placed the modules on a 2–axis solar tracker and modified manually the inclination in order to obtain the desired value of G on the module plane. For each module, a value of G as close as possible to the value of the 1996 measurement was selected. In addition, several curves were measured at different cell temperatures, with the procedure described in detail in Section 3.5, so that also the value of the temperature could be chosen to be as close as possible to the one of the 1996 measurement. This procedure was used to minimize the errors associated to the *I*–*V* curve translation process.

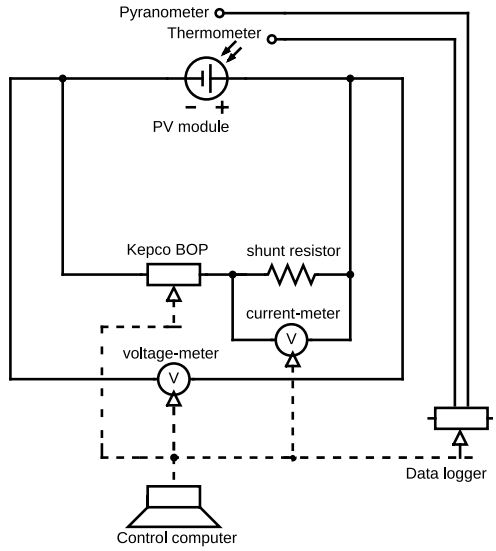

FIGURE 1 Schematic block diagram of the measurement system layout.

Instead of using a commercial *I*–*V* curve tracer, we have designed our own system [14], based on several laboratory instruments connected to a computer that commands all of them. A bipolar 4–quadrant power supply is used to bias the operating point of each PV module gradually between the short–circuit and the open–circuit states while the current–voltage points are measured by means of two high–precision multimeters using a four–wire connection as it can be seen in Figure 1. The current is obtained by the measurement of the voltage drop across the shunt resistor. The measured data are retrieved from the internal memory of the multimeters by the computer and the *I*–*V* curve is stored in a database. Subsequently, it is possible to access and download the measured *I*–*V* curves through a WEB platform accessible from any computer with internet access [15]. The main differences between the instruments used at the beginning (1996) and at the end (2017) of the exposure period are summarized in Table 5 (the measurement system in 2008 is exactly the same from 2017 except for not yet having replaced the pyranometer used in 1996).

Function	**1996**		**2017**	
Bipolar Power Supply	Kepco BOP 100-4M -	V_{range} = ±100 V I_{range} = ±4 A	Kepco BOP 100-10MG	V_{range} = ±100 V I_{range} = ±10 A
Voltage meter	Fluke 8842A [16]	V_{range} = ±200 V 100 readings/s A/D: n = 16 bit	Agilent 34411A [17]	V_{range} = ±100 V 300 readings/s A/D: n = 22 bit
Current meter*	Fluke 8842A [16]	V_{range} = ±200 mV 100 readings/s A/D: n = 16 bit	Agilent 34411A [17]	V_{range} = ±100 mV 300 readings/s A/D: n = 21 bit
Shunt resistor	Kainos	4A / 150mV class 0.5	Celsa	10A / 100mV class 0.1
Pyranometer	Kipp & Zonen	CM21 [18]	EKO	MS–80A [19]
Thermometer	thermo–couple TC	type-K	thermo–resistance RTD	Pt100 class B
Data logger	Fluke Hydra ch. G : mode VDC ch. T : mode °C	2625A [20] V_{range} = ±300 mV TC type: K	National Instruments ch. G : mode ADC ch. T : mode °C	Compact FieldPoint [21] I_{range} = 4 – 20 mA RTD type: Pt100

* The current is sensed by the voltage drop across the shunt resistor

TABLE 5 Different sensors and instruments used in 1996 and 2017.

For estimating the electrical parameters, the procedure described by Emery [22] is followed. For I_{SC} and V_{OC}, linear regressions can be performed using a selection of points around $V = 0.0$ V and $I = 0.0$ A respectively (see Table 6). The slopes of the regression lines are also estimated ($R_{s0} = -\left.\frac{dV}{dI}\right|_{I=0}$ and $R_{sh0} = -\left.\frac{dV}{dI}\right|_{V=0}$). In order to determine P_{max}, a fifth–degree polynomial is fitted to the points in the range specified in Table 6, and V_{Pmax} is set to be the real value that makes zero the first derivative of this polynomial. Substituting this value in the polynomial gives us P_{max}, and $I_{Pmax} = \frac{P_{max}}{V_{Pmax}}$. In Table 6, I_0 is the current value of the closest point to the $V = 0.0$ V axis, V_0 is the voltage value of the closest point to the $I = 0.0$ A axis, and P_0 is the power value of the discrete point with maximum product $I(i) \cdot V(i)$.

Parameter	Min. voltage	Max. voltage	Min. current	Max. current	Min. power	Max. power
I_{SC}	0.0 V	$0.20 \cdot V_0$	$I_0 - 0.04 \cdot I_0$	$I_0 + 0.04 \cdot I_0$		
V_{OC}	$V_0 - 0.10 \cdot V_0$	$V_0 + 0.10 \cdot V_0$	$-0.20 \cdot I_{SC}$	$+0.20 \cdot I_{SC}$		
P_{max}					$0.85 \cdot P_0$	$1.00 \cdot P_0$

TABLE 6 Ranges for selecting the points to determine I_{SC}, V_{OC}, and P_{max} using regression.

In order to estimate the parasitic resistances of each module, a curve fitting procedure to the double–diode model (DDM) equation was followed [23]. This model is described by (eq. 1):

$$I = I_{ph} - I_{s_1}\left[\exp\left(\frac{V + IR_s}{V_t}\right) - 1\right] - I_{s_2}\left[\exp\left(\frac{V + IR_s}{2V_t}\right) - 1\right] - \frac{V + IR_s}{R_{sh}} \tag{1}$$

where I and V are the output current and voltage, $V_t = N_s kT/q$ is the thermal voltage of the module (being T the temperature in kelvin, N_s the number of cells in series, k is the Boltzmann constant, and q is the elementary charge), I_{ph} is the photo–induced current, R_s is the series resistance, R_{sh} is the parallel resistance, and $\{I_{s_1}, I_{s_2}\}$ are the dark saturation currents of the diodes. Therefore, there are 5 parameters to be identified. These are shown in Table 7, together with the search space and the guess solution required by the trust–region algorithm, a non–linear curve–fitting tool which was implemented in Matlab [24].

	I_{ph}	I_{s_1}	I_{s_2}	R_s	R_{sh}
unit	A	A	A	Ω	Ω
Interval	[0.1, 10]	[1e-12, 1e-5]	[1e-9, 1e-3]	[0, 5]	[50, 500]
Initial	I_{SC}	5e-6	5e-4	R_{s0}	R_{sh0}

TABLE 7 Feasible region and guess solution for the curve–fitting tool.

2.2 | Applying *"procedure 1"* of the IEC 60891 standard

For each PV module measured in the year 1996, we have an *I*–*V* curve measured at an irradiance G_1 and module temperature T_1. In 2017, we have performed several measurements under the same irradiance and within a range of temperatures wide enough. Then, it is possible to select among all the *I*–*V* curves of 2017 that one with T_2 closest to T_1 (and with a value G_2 similar to G_1). Even so, there will be a small difference between both set of conditions. The *"procedure 1"* of the IEC 60891 [25] allows us to correct measured *I*–*V* curves to other conditions, using the series resistance R_s and the temperature coefficients α, β and κ, provided by the manufacturer. Instead of correcting both curves to a fixed set of reference conditions (applying twice *procedure 1*), we have decided to correct only each individual *I*–*V* curve measured in 1996 to the exact conditions of the selected curve measured in 2017. In such a way, only the curve measured in 1996 is corrected, and the curve from 2017 is exactly the measured one.

Let $\{(V_1^{(1)}, I_1^{(1)}), \ldots, (V_1^{(m)}, I_1^{(m)})\}$ be an I–V curve with m points measured at an irradiance G_1 and module temperature T_1 (with a short–circuit current $I_{SC,1}$). In order to calculate the corrected curve $\{(V_2^{(1)}, I_2^{(1)}), \ldots, (V_2^{(m)}, I_2^{(m)})\}$ that corresponds to G_2 and T_2, each point $(V_1^{(j)}, I_1^{(j)})$ of the first curve is translated to the point $(V_2^{(j)}, I_2^{(j)})$ of the second curve following (eq. 2) and (eq. 3):

$$I_2^{(j)} = I_1^{(j)} + I_{SC,1} \cdot \left(\frac{G_2}{G_1} - 1\right) + \alpha(G_2) \cdot (T_2 - T_1) \tag{2}$$

$$V_2^{(j)} = V_1^{(j)} - R_s(T_1) \cdot (I_2^{(j)} - I_1^{(j)}) - \kappa \cdot I_2^{(j)} \cdot (T_2 - T_1) + \beta \cdot (T_2 - T_1) \tag{3}$$

The values for β and κ that appear in Table 2 can be used directly. However, as it is highlighted by King et al. [26], α depends linearly on the level of irradiance, in such a way that its value (usually reported at STC) must be scaled by (eq. 4) to the target irradiance G_2 before being used:

$$\alpha(G_2) = \alpha_{SCT} \cdot \left(\frac{G_2}{G_{STC}}\right) \tag{4}$$

Analogously, R_s depends non–linearly on the temperature [27], although in a narrow range of operation, this dependency can be assumed to be linear. Therefore, the value $R_{s,STC}$ cannot be used directly in (eq. 3). This previous value should be corrected to T_1 using (eq. 5):

$$R_s(T_1) = R_{s,STC} + \kappa \cdot (T_1 - T_{STC}) \tag{5}$$

2.3 | Analysis of uncertainty

According to ISO/IEC Guide 98-3 [28], and taking into account the specifications in terms of accuracy of the instruments used in 1996 and in 2017, the type–B uncertainty of a single measurement of voltage and current is determined. For measuring the current–voltage pairs, 1–year time span from the last calibration is assumed, maximum reading speed is set, and no temperature drift correction is applied. For the irradiance and cell temperature measurements, the data logger is set at the minimum reading rate in order to increase the measurement accuracy. For all the instruments, we have assumed a Tolerance Uncertainty Ratio (TUR) of 4:1. By applying the approach described by Whitfield and Osterwald [29], it is possible to calculate the expanded uncertainty for a single voltage measurement V in 1996 and 2017 using (eq. 6) and (eq. 7), and for a single current measurement I using (eq. 8) and (eq. 9):

$$U_V^{1996} = 2 \cdot \sqrt{4.3\text{e}{-10} \cdot V^2 + 4.9\text{e}{-8} \cdot |V| + 1.4\text{e}{-6}} \tag{6}$$

$$U_V^{2017} = 2 \cdot \sqrt{5.6\text{e}{-10} \cdot V^2 + 5.9\text{e}{-8} \cdot |V| + 1.5\text{e}{-6}} \tag{7}$$

$$U_I^{1996} = 2 \cdot \sqrt{8.3\text{e}{-6} \cdot I^2 + 2.6\text{e}{-8} \cdot |I| + 1.0\text{e}{-7}} \tag{8}$$

$$U_I^{2017} = 2 \cdot \sqrt{3.3\text{e}{-7} \cdot I^2 + 6.5\text{e}{-8} \cdot |I| + 1.2\text{e}{-6}} \tag{9}$$

Finally, the expanded uncertainty (95% of confidence; coverage factor $k = 2$) associated to the individual power at a point (V, I) can be estimated by applying the uncertainty propagation rule [28] leading to (eq. 10) and (eq. 11):

$$U_P^{1996} = 2\sqrt{8.3\text{e-}6 I^2 V^2 + 4.9\text{e-}8 I^2 |V| + 1.4\text{e-}6 I^2 + 2.6\text{e-}8 V^2 |I| + 1.0\text{e-}7 V^2} \tag{10}$$

$$U_P^{2017} = 2\sqrt{3.3\text{e-}7 I^2 V^2 + 5.9\text{e-}8 I^2 |V| + 1.5\text{e-}6 I^2 + 6.5\text{e-}8 V^2 |I| + 1.2\text{e-}6 V^2} \tag{11}$$

The uncertainties of I_{SC} and V_{OC} are calculated by taking into account that both are estimated by means of a linear regression. The procedure used to estimate P_{max} described by Emery [22] involves an iterative procedure with its own fitting uncertainty. In any case, the uncertainty of a single measurement should be combined with the uncertainty of the intercept in a linear regression as it can be seen in (eq. 12).

$$U_{I_{SC}} = 2\sqrt{\left(\frac{U_I(I_{SC})}{2}\right)^2 + (u_{I\text{-}fit})^2} \quad U_{V_{OC}} = 2\sqrt{\left(\frac{U_V(V_{OC})}{2}\right)^2 + (u_{V\text{-}fit})^2} \quad U_{P_{max}} = 2\sqrt{\left(\frac{U_P(P_{max})}{2}\right)^2 + (u_{P\text{-}fit})^2} \tag{12}$$

The value of $U_I(I_{SC})$ is determined by applying (eq. 8) or (eq. 9) to the estimation of I_{SC}. Analogously, $U_V(V_{OC})$ and $U_P(P_{max})$ can also be calculated. For a simple linear regression, the uncertainty of the intercept can be estimated from the coefficient of determination R^2 [30] as it is indicated in (eq. 13), where m is the number of selected points. However, in the case of $u_{P\text{-}fit}$, it is more complicated, but Emery [22] provides a relative expanded uncertainty of 0.06% (which means that $u_{P\text{-}fit} = (0.0006/2) \cdot P_{max}$).

$$u_{I\text{-}fit} = \frac{1}{R_{sh0}}\sqrt{\frac{1/R^2 - 1}{m-2} \cdot \frac{\sum_{k=1}^{m} V_k^2}{m}} \qquad u_{V\text{-}fit} = R_{s0}\sqrt{\frac{1/R^2 - 1}{m-2} \cdot \frac{\sum_{k=1}^{m} I_k^2}{m}} \tag{13}$$

On the one hand, the expanded uncertainty associated to an estimation of the fill factor FF is a direct application of the propagation rule [14]. On the other hand, when identifying the values of R_s and R_{sh} using the trust–region method, the own algorithm [24] returns as an optional output an uncertainty interval for each parameter (95% confidence level).

The uncertainty of a reading of irradiance is estimated following the work of Kratzenberg et al. [31]. In addition to the resolution, the measurement error and the calibration error of the multimeter (combined in the expanded uncertainty U_{Gm}), as well as other several sources of uncertainty related to the pyranometer must be considered, such as the directional error and the spectral sensitivity, among others (combined in the expanded uncertainty U_{Gp}). Finally, some pyranometers include an internal signal conditioner (from mV to 4–20 mA). In the case of the one used in 2017, this implies a maximum error $e_{sc} = 1.7$ W/m^2 at 1 SUN [19]. The global expanded uncertainty U_G (95% confidence level; coverage factor $k = 2$) is the result of combining previous ones and it is reported in Table 8 for 1996 and 2017 for a value of G around 1 000 W/m^2.

In order to estimate the uncertainty of T, the most important term is the maximum error of the specific type of sensor e_{ts} (2.2 °C in 1996 for a type–k thermocouple [32] and 0.6 °C in 2017 for a RTD Pt100 class B [33]). Other sources of error related to the data logger resolution, accuracy and calibration, are also taken into account to estimate the expanded uncertainty of temperature due to the data logger U_{tm}. In addition, as we are not measuring the actual cell temperature (the sensor is attached to the back module surface), a last source of uncertainty $e_\Delta = 1$ °C must to considered [14]. Finally, assuming a reading of $T \in (40, 50)$°C, the expanded uncertainty U_T (95% confidence level; coverage factor $k = 2$) for 1996 and 2017 can be seen in Table 8

Year	$U_{Gm}(k=2)$	$U_{Gp}(k=2)$	$U_{e_{sc}}(k=\sqrt{3})$	$U_G(k=2)$	$e_{ts}(k=\sqrt{3})$	$U_{tm}(k=2)$	$e_\Delta(k=\sqrt{3})$	$U_T(k=2)$
1996	2.3 W/m^2	30 W/m^2	–	30 W/m^2	0.8 °C	2.2 °C	1.0 °C	3 °C
2017	2.3 W/m^2	15 W/m^2	1.7 W/m^2	15 W/m^2	0.7 °C	0.6 °C	1.0 °C	1.5 °C

TABLE 8 Sources of error and expanded uncertainties for irradiance and cell temperature measurements.

Finally, the uncertainty of the individual measured I–V pairs will be propagated when using the *procedure 1* of the IEC 60891 [25]. To rigorously quantify this uncertainty, it would be required to know the uncertainty of the temperature coefficients and the series resistance. Although we do not have those uncertainties for this specific PV module, Dirnberger et al. [34] provides these generic conservative values of relative standard uncertainty: $u_\alpha = 25\%$, $u_\beta = 10\%$, and $u_{R_s} = 5\%$. Applying the rule of propagation of the uncertainty to (eq. 2) and (eq. 3) two expressions are obtained for the uncertainty for an individual corrected I–V pair, but assuming $G_1, G_2 \in (950, 1050)$ W/m^2 and $(T_2 - T_1) \leq 5$ °C, some terms can be neglected obtaining (eq. 14) and (eq. 15) for obtaining the expanded uncertainty (95% confidence level; coverage factor $k = 2$) of the corrected I–V pairs. Once the corrected I–V curve has been obtained, the main electrical parameters and their uncertainties should be again estimated.

$$U_{I\text{-}corr} = 2 \cdot \sqrt{\left(\frac{U_I(I_1^{(j)})}{2}\right)^2 + \left(\frac{I_{SC,1} \cdot G_2}{G_1^2} \cdot \frac{U_{G_1}}{2}\right)^2 + \left(\frac{I_{SC,1}}{G_1} \cdot \frac{U_{G_2}}{2}\right)^2 + \left((T_2 - T_1) \cdot u_{\alpha_{STC}}\right)^2} \tag{14}$$

$$U_{V\text{-}corr} = 2 \cdot \sqrt{\left(\frac{U_V(V_1^{(j)})}{2}\right)^2 + \left(R_s(T_1) \cdot \frac{U_I(I_1^{(j)})}{2}\right)^2 + \left(R_s(T_1) \cdot \frac{U_I(I_2^{(j)})}{2}\right)^2 + \left((I_2^{(j)} - I_1^{(j)}) \cdot u_{R_s}\right)^2 + \left(\beta \cdot \frac{U_{T_1}}{2}\right)^2 + \left(\beta \cdot \frac{U_{T_2}}{2}\right)^2 + \left((T_2 - T_1) \cdot u_\beta\right)^2} \tag{15}$$

3 | RESULTS

3.1 | Visual inspection

The selected PV modules have been disconnected and uninstalled from the solar generator. After a deep cleaning, they have been visually inspected and the different types of faults have been identified (see Figure 2) and classified (see Table 9). The classification proposed in this paper is similar to others proposed in the literature [2, 6, 9, 35].

type	description	figures	#1	#2	#3	#4	#5	#6	#7	#8	#9	#10
T1	**Glass break**	–	0	0	0	0	0	0	0	0	0	0
T2	**Permanent soiling**	(2a)	1	1	1	1	2	1	1	1	1	2
T3	**Connection–box anomalies**	(2b),(2c)	1	2	1	1	1	1	1	1	1	2
T4	**Frame corrosion**	(2d)	1	1	1	1	1	1	1	1	1	1
T5a	**EVA bubbles**	–	0	0	0	0	0	0	0	0	0	0
T5b	**EVA milky pattern**	(2e)	1	0	0	0	1	2	2	2	0	0
T5c	**EVA browning**	(2f)	1	1	1	1	2	2	1	2	1	1
T6	**Back–layer detachment**	(2g), (2h)	1	2	2	0	2	0	0	0	0	2
T7	**Bus–bars corrosion**	(2i)	1	2	1	1	2	2	1	2	1	1
T8	**Cell cracking**	(2i),(2j),(2l)	1	2	2	1	2	2	1	2	2	1
T9	**Burned cell**	(2k),(2l)	0	0	2	0	0	0	2	0	0	0

0 means no problem / 1 means moderate presence of the problem / 2 means severe problem

TABLE 9 Valuation of the presence of the different problems in the PV modules.

(a) Permanent soiling - T2 - mod#5
(b) Wasp nest in box - T3 - mod#7
(c) Burned cable in box - T3 - mod#2
(d) Frame corrosion - T4 - mod#1
(e) Milky pattern - T5b - mod#6
(f) EVA browning - T5c - mod#8
(g) Tedlar delamination - T6- mod#2
(h) Tedlar delamination - T6 - mod#10
(i) Corrosion/cell crack- T7,T8 - mod#5
(j) Cracked cell - T8 - mod#2
(k) Burned cell - T9 - mod#3
(l) Burned/cracked cell - T8,T9 - mod#7

FIGURE 2 Result of the visual inspection of the modules under study.

All the PV modules present a permanent soiling band (defect T2, Figure 2a) between the edge of the lower frame and the row of cells closest to that side. Since the distance between the frame and the first row of the cells is very small in the module type I–53, this could have consequences on the electrical behavior. However, it is not sufficient to generate a clear step in the *I*–*V* curves as a consequence of the activation of a by–pass diode, as it can be seen in Figure 3. This is a typical defect on modules operating for long periods of time [6, 36, 37]. This anomaly is significantly more intense in modules #5 and #10, that are the only ones with burned cables (defect T3, Figure 2c). Burned cables and defective boxes are much more common than one might expect [38]. All the modules present detachment of the screw terminal block inside the connection box (classified as T3 and also reported in the literature [39]).

All the PV modules have a slight level of frame corrosion (defect T4, Figure 2d). This could be considered a security risk, but according to previous findings [40], its impact on the electrical performance can be neglected. In many cases, the back layer surface has been partially detached (defect T6, Figures 2g and 2h). This defect has been reported also in previous works [2, 9, 41]. Another type of defect, which is not present the in all the modules is T5b (known as milky pattern [6, 9]), being more intense in modules numbers #6, #7 and #8.

However, there are other visual defects (T5c, T7, T8 and T9) which are more important from the point of view of the degradation of the energy output of the modules. All the modules, suffer browning of the EVA layer (defect T5c, which results in a bicolor pattern (Figure 2f) and an important loss of transparency identified in previous works [39, 42] and analyzed in depth by Kaplanis and Kaplani [43]. In addition, there is a presence of corrosion of the interconnecting ribbons in all the modules (defect T7 also documented by Sastry et al. [39], Figure 2i). This last defect implies an increase in the series resistance of all the modules. There are also a large number of visible cell cracks in every module (defect T8, Figure 2j). This problem and its effect on the electrical performance is studied by Dhimish et al. [44]. Two modules have a cell that is completely burned (modules #3 and #7, as it can be seen in Figures 2k and 2l respectively). This phenomenon has been also identified by Köntges et al. [2]. In both modules there is a loss of transparency of the EVA between the glass and the cell. Nevertheless, both modules are operational, and as it will be evident hereafter, the consequences have not been as severe as it might have been expected.

3.2 | Main electrical parameters

For each module, two *I*–*V* curves are shown in Figure 3: the one measured in 1996 and one measured in 2017 at an irradiance and temperature conditions that are the closest to the conditions of the former curve of 1996, which has also been translated to the conditions of the curve acquired in 2017. For each module, the values of P_{max}, I_{SC}, V_{OC} are shown, both for the curve of 1996 (corrected to the conditions in 2017) and the measured one of 2017. In addition, an annual degradation rate is provided for each parameter.

In the case of P_{max}, the annual degradation for almost all the modules is around 0.9%, but modules #2 and #9 have only a degradation rate slightly higher than 0.8%. This result is in line with the values reported in the previous work over the modules of the same installation nine years before [6]. In addition, other works in the literature estimate similar annual degradation rates in terms of power for mc–Si modules [4, 7, 45, 46]. Comparing these numbers with the data in Table 9, we see that the two modules with burned cells (modules #3 and #7) have degraded in terms of power similarly to the others. On the one hand, the modules that present the best visual appearance (modules #1 and #4) have not experienced lower drops in P_{max} (see Table 10). On the other hand, module #3, which is one of those with a burned cell and an overall poor appearance, is surprisingly one of the modules with the lowest power degradation rate.

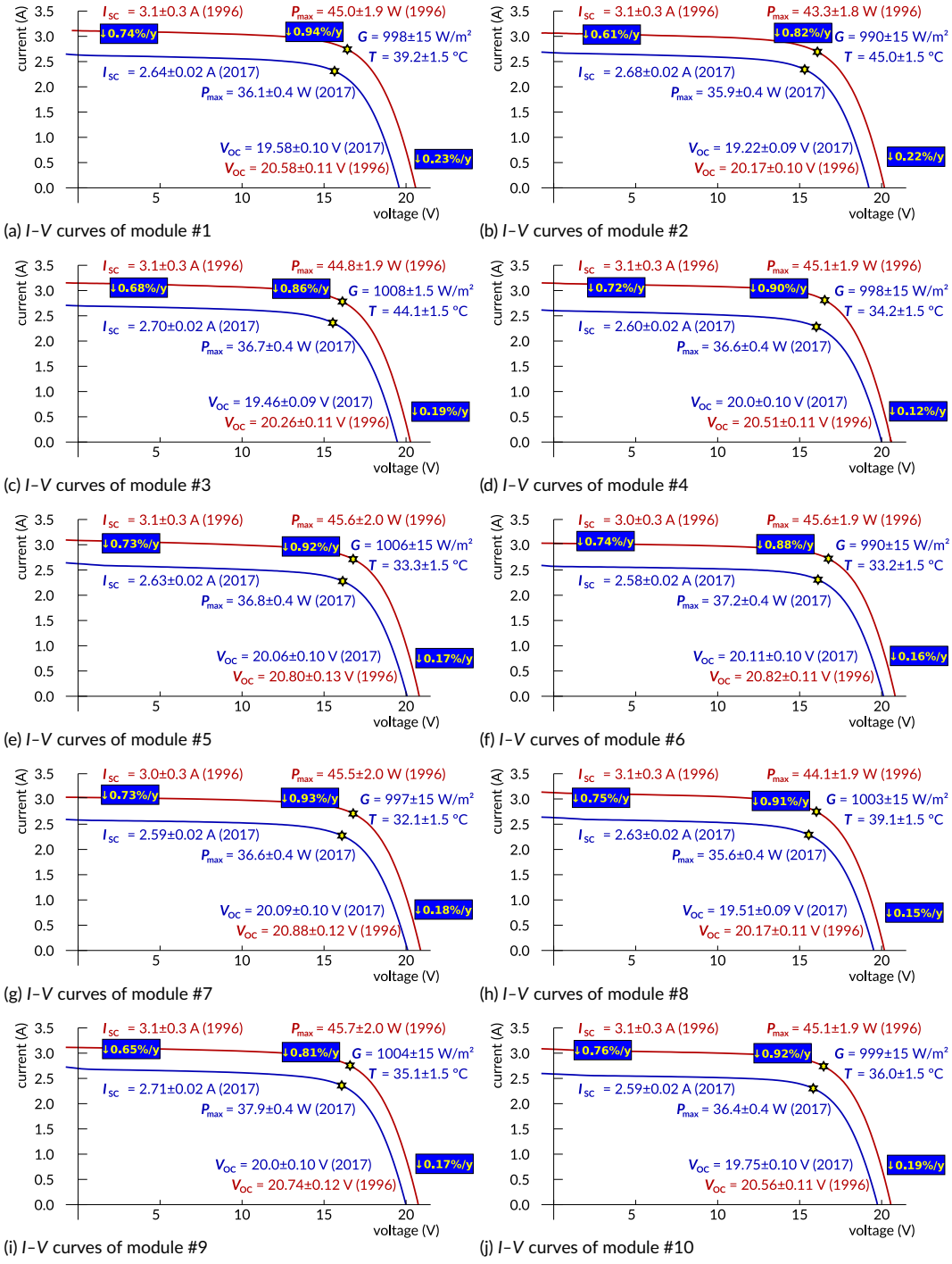

FIGURE 3 Analysis of the curves measured in 2017 and the curves of 1996 corrected to the conditions in 2017 (given at the upper–right corner of each sub–figure)

Clearly, the main contributor factor in the power annual degradation rate is the decrease of the short–circuit current. For almost all the modules, the annual degradation rate in terms of I_{SC} is around to 0.7%, ranging from 0.65%/year to 0.76%/year. This relative small dispersion means that all the modules have degraded their I_{SC} in a similar way. This decrease in current might be a consequence of the reduction of the number of photons able to reach the p–n junction. It is mainly related to the loss of transparency of the encapsulating materials, which is evident by the visual inspection. Regarding to the cover glass, in the visual inspection, defect T2 (permanent soiling) is present in all the modules. In addition, as it is stated by Sánchez–Friera et al. [6], the loss of transparency is not equal for all the wavelengths, so that the glass becomes more spectral selective while ageing.

Other element that has a strong impact in the decay of the current is the alterations observed in the EVA layer. Some of these defects, as EVA milky pattern (type T5b), affect only small areas of the cell, whereas other defects, such as the browning (type T5c) cover all the area of the cell. Doumane et al. [47] highlight the important impact of EVA browning (that is present in all the studied modules) on the reduction of the energy output. A last cause of this photon number reduction could be the degradation of the anti–reflective coating of the cells, that can reduce its effectiveness throughout time. Therefore, the angular losses are more critical as the module ages, considerably reducing the energy produced in the first and last hours of the day.

In terms of the open–circuit voltage, also all the PV modules have experienced a slight drop. This decrease of V_{OC} ranges between 0.12%/year and 0.23%/year. This range is specially wide, implying that the degradation of this parameter is very different among the set of modules. The modules #1 and #2 are the ones with the highest V_{OC} degradation, but analyzing Table 9, it is not possible to find any visual signs which are significantly different in these modules with respect to the others. Köntges et al. [2] state that the main reasons for this type of degradation are the formation of short circuits between the cells or else failure of the bypass diodes. Other possible causes could be an increase of the cell parameters mismatch or long–term effects on the p–n junction. More advanced diagnosis techniques would be required in order to identify the cause of this voltage drop.

3.3 | Fill factor and parasitic resistances

Other parameters that could be interesting to compare between 1996 and 2017 are the fill factor FF and the parasitic resistances: the series resistance R_s and the parallel resistance R_{sh}. Table 10 shows the results obtained for the PV modules under study. The expanded uncertainties of the values of FF have been calculated as explained in Section 2.3. In contrast, the uncertainties of the values of R_s and R_{sh} have been returned as an additional output of the curve–fitting routine from Matlab [24] (95% of confidence level).

At a first glance, it could seem that there was an overall reduction of the FF for the ten PV modules under study when comparing the curves measured in 1996 to the ones measured in 2017. However, the problem is that the uncertainty in the estimation of this parameter (around 1%) is higher than the possible variation. In all cases the confidence intervals of the values to compare overlap, so it is not possible to state that there has been a real decrease of the value. In the literature there are contradictory statements about this parameter: whereas Bouaichi et al. [48] claim that there is no variation, other authors report different significant rates of degradation depending on the climatic

conditions [49].

	Module #1			Module #2		
	1996	**2017**	**% annual**	**1996**	**2017**	**% annual**
FF (%)	70.4±1.1	70.3±1.0	**0.0**	70.1±1.1	69.9±1.1	**0.0**
R_s (Ω)	0.341±0.005	0.374±0.007	**+0.46**	0.340±0.005	0.368±0.004	**+0.39**
R_{sh} (Ω)	146±9	145±11	**0.0**	141±8	136±6	**−0.1**
	Module #3			Module #4		
	1996	**2017**	**% annual**	**1996**	**2017**	**% annual**
FF (%)	70.3±1.1	69.9.3±1.0	**0.0**	71.8±1.1	70.2±1.0	**−0.1**
R_s (Ω)	0.347±0.006	0.364±0.009	**+0.24**	0.366±0.013	0.406±0.010	**+0.52**
R_{sh} (Ω)	139±10	134±13	**−0.2**	184±24	124±10	**−1.5**
	Module #5			Module #6		
	1996	**2017**	**% annual**	**1996**	**2017**	**% annual**
FF (%)	70.9±1.1	70.1±1.0	**0.0**	72.1±1.1	72.0±1.1	**0.0**
R_s (Ω)	0.339±0.011	0.400±0.011	**+0.86**	0.357±0.013	0.424±0.009	**+0.89**
R_{sh} (Ω)	113±9	108±10	**−0.2**	268±33	240±38	**−0.5**
	Module #7			Module #8		
	1996	**2017**	**% annual**	**1996**	**2017**	**% annual**
FF (%)	71.4±1.1	70.6±1.0	**−0.1**	70.0±1.1	69.5±1.1	**0.0**
R_s (Ω)	0.359±0.013	0.404±0.012	**+0.60**	0.344±0.008	0.391±0.012	**+0.66**
R_{sh} (Ω)	187±26	178±30	**−0.2**	155±13	138±17	**−0.5**
	Module #9			Module #10		
	1996	**2017**	**% annual**	**1996**	**2017**	**% annual**
FF (%)	70.8±1.1	70.7±1.0	**0.0**	71.4±1.1	71.4±1.1	**0.0**
R_s (Ω)	0.366±0.010	0.374±0.014	**+0.11**	0.364±0.018	0.399±0.013	**+0.46**
R_{sh} (Ω)	145±21	123±17	**−0.7**	242±39	213±46	**−0.6**

TABLE 10 Comparative of R_s and R_{sh} between 1996 and 2017.

Something similar occurs when analyzing the identified values of R_{sh} in 1996 and in 2017. The confidence interval of this parameter provided by the curve–fitting procedure is very sensible to the measurement noise, in such a way that the estimated confidence interval is too wide, especially in some cases. This implies that we cannot establish whether or not the value of R_{sh} has experienced a real variation during the 21 years of exposure. Very similar results are achieved by Reis et al. [50], where there is also a high uncertainty in the estimations. An exception to the previous discussion occurs for module #4, in which the decrease of R_{sh} in 2017 with respect to that of 1996 is still much greater than the uncertainty in both measurements. This module had to have some individual problem that explains this abrupt drop, perhaps a faulty isolation issue. However, taking into account its visual aspect (see column #4 in Table 9), it is one of the modules in best visual conditions, having the back sheet layer in perfect condition (contrary to some other modules where it is detached partially or totally).

The only parameter of Table 10 that experiences an increase between 1996 and 2017 is R_s. In almost all the cases, the rate of increment of R_s is significant (higher than 0.4%/year and much more). Previous literature agrees with our results in terms of R_s [50, 51]. Only in two cases (modules #3 and #9), the annual degradation rates in terms of R_s could be considered low or even negligible. As all the cells are connected in series, the increment of the series resistance could be due to a generalized increment of this parameter in every cell, or else, due to the contribution of only one cell with an abnormal high resistance [2]. However, other causes of this degradation could be the corrosion of the interconnection tabs or the soldering points. Even a failure in the connection box could represent a great increment of R_s. From the results, the three modules with the highest increment of R_s are #5, #6 and #8; if Table 9 is considered, these modules are the group of those with the highest degree of corrosion in the bus–bars. It is easy to see without special cameras that not all the modules present the same level of corrosion, and this could be an explanation of the dispersion in the values of R_s and also of the different annual degradation rates that we have obtained.

3.4 | Mean results in both exposure periods

The intermediate values obtained in 2008 allow us to know if the degradation processes are uniform or, in contrast, if the process has been accelerated at the last period. For each main electrical parameter, I_{SC}, V_{OC} and P_{max}, and for the series and shunt resistances (R_s and R_{sh}) the mean annual degradation rates (among the 10 modules under study) corresponding to the first period (12 years), to the second period (9 years) and to the total period (21 years) are summarized in Table 11 (next to the corresponding standard deviation). The values of other analyzed parameters (FF and R_{sh}) have not been included because the uncertainty in their determination is very high with respect the observed change.

	years	P_{max}	I_{SC}	V_{OC}	R_s
First period (from 1996 to 2008)	12	−0.91±0.07%	−0.73±0.06%	−0.16±0.05%	+0.52±0.28%
Second period (from 2008 to 2017)	9	−0.87±0.06%	−0.68±0.08%	−0.17±0.07%	+0.53±0.27%
Total period (from 1996 to 2017)	21	−0.89±0.05%	−0.71±0.05%	−0.18±0.03%	+0.52±0.25%

TABLE 11 Mean annual rates of degradation at different periods of time

As it can be seen from these results and analyzing only the ten PV modules under study, in terms of maximum power, the mean annual degradation rate during the first period of exposure (0.91%/year from 1996 to 2008) is only a bit greater than the equivalent rate for the second period (0.87%/year from 2008 to 2017). This discrepancy is not significant if the standard deviations of both mean values are taken into account. The mean values of the degradation rates of the I_{SC} between the first 12 years and the following 9 years are also very close (0.73%/year versus 0.68%/year), also smaller than the standard deviation. Similar findings are obtained for the degradation of V_{OC} throughout both periods of exposure. Although from the results a linear degradation pattern can be inferred, a simulation performed by Nehme [52] suggests that the performance and efficiency follow an inverse–exponential behavior throughout the years. Finally, it must be highlighted that the values of the degradation rates of the ten modules under study show an abnormally high standard deviation. This could be partly due to the dispersion of the R_s degradation, or also, the high uncertainty of the method used to determine the values of R_s.

3.5 | Degradation of the temperature coefficients

Finally, the temperature coefficients α, β, and γ of the degraded PV modules have been determined and compared to the nominal values declared by the manufacturer. Initially, each PV module to be measured is covered by an opaque frozen–gel wrap that is removed just before starting the acquisition of a sequence of I–V curves. Due to a natural effect of the incident radiation from the Sun, the module temperature increases, in such a way that each curve is measured at a higher temperature than the previous one. During the measurement, it is necessary to maintain the irradiance level as constant as possible and around 1 000 Wm^{-2}. A linear regression is performed to fit the plot of each electrical parameter versus the module temperature. The slope of the regression line is the temperature coefficient. The results are summarized in Table 12, where, in addition, the mean values of the 10 modules temperature coefficients and the nominal values are shown.

	I–53	#1	#2	#3	#4	#5	#6	#7	#8	#9	#10	Mean	Annual
α (mA/°C)	**1.29**	0.94	1.02	0.99	1.00	0.90	0.89	1.07	1.07	0.95	1.11	**0.99**	**−1.1%**
β (mV/°C)	**−80**	−81	−81	−75	−77	−78	−71	−74	−72	−79	−79	**−77**	**−0.2%**
γ (mW/°C)	**−256**	−189	−194	−192	−178	−182	−170	−168	−163	−185	−184	**−181**	**−1.4%**

TABLE 12 Temperature coefficients of the modules at STC after 21 years of operation.

The values of α of the degraded modules range between 0.98 and 1.11 mA/°C, with a mean value of 0.99 mA/°C, thus showing either a significant decrease with respect the nominal value 1.29 mA/°C with a relative reduction greater than 1.1% per year, or else, a discrepancy between the real values of α and the nominal ones provided by the manufacturer for a module type and not for a specific specimen. In any case, it is a safer procedure to recalculate the values of α when intending to apply the IEC 60891 [25] *procedure 1* to the *I–V* curve of a degraded module. Remember that in this work, the nominal values have been used only to correct the *I–V* curve measured in 1996 when the module was not degraded (the curves of 2017 have not been corrected).

As proposed by Emery et al. [53], each temperature coefficient can be reported using its normalized value, dividing by its respective electrical parameter at STC. In our case, the value of α of a degraded module should be divided by I_{SC} at STC, also in degraded condition. The mean value of this normalized α_{rel} among the 10 modules (with the standard deviation) is 0.038±0.003%/°C, whereas for a new module is 0.039%/°C. This means that the normalization of the temperature coefficient cancels what might be due to degradation.

Focusing on the evolution of the temperature coefficient β, from the obtained results, we are not able to state that its value has changed through time. As it can be seen in Table 12, β varies from −81 to −71 mV/°C, with a mean value of −77 mV/°C. However, the nominal value stated by the manufacturer $\beta = -80$ mV/°C, is practically the same obtained for the degraded modules. As in the case of α, it is also possible to obtain β_{rel} obtaining a mean value for all the modules of 0.37 %/°C.

The temperature coefficient γ, after 21 years of exposure, shows a significant reduction of its absolute value, from a nominal value of −256 mW/°C to a mean value for the degraded PV modules of −181 mW/°C, between −194 and −163 mW/°C, thus resulting in an annual rate of decrease of 1.4%. However, if the normalized value is taken into account, we obtain a mean value and a standard deviation of $\gamma_{rel} = -0.46 \pm 0.02$ %/°C, perfectly matching to the nominal value also normalized (−0.48 %/°C), cancelling also the effect of degradation. These obtained results about the relative temperature coefficients agree with Mitterhofer et al. [54], who state that these normalized temperature coefficients only experiment a seasonal change, but they do not vary in the long term. In contrast, Berthod et al. [55], find that PV module degradation could produce a decrease of the absolute values of α_{rel}, β_{rel} and γ_{rel}. Therefore, these issues are still an open field of study and analysis.

4 | CONCLUSIONS

The visual analysis performed shows a great variety of defects. Despite this fact, all the PV modules are operational. Some common defects do not lead to important effects on the electrical performance, such as permanent soiling, detachment of the screw terminal block, corrosion of the frame or back layer surface detachment. However, other visual defects can have a larger influence on the energy output. This is the case for EVA browning, corrosion of the bus–bars and burned or cracked cells. Our analysis has shown, however, that very often there is no clear correlation between the observed visual defects and the PV module electrical performance. Modules with severe visual defects can show low degradation rates and conversely, modules with a lower amount of visual defects can show large decays in their electrical performance.

For each module, a comparison has been performed between a curve measured in 1996 and another one from 2017. The annual degradation rates of P_{max}, I_{SC} and V_{OC}, have been estimated and the mean values over the set of modules have been obtained: 0.89%/year for P_{max}, 0.71%/year for I_{SC}, and 0.18%/year for V_{OC}. Taking into account an intermediate measurement point in 2008, these degradation rates seem to be linear throughout time.

Additional analysis about R_s reveals that between 1996 and 2017, a significant increase has happened with a mean value of 0.52%/year. In this case, there seems to be a clear relationship between this increment and the corrosion level of the bus–bars and interconnection ribbons. Regarding FF and R_{sh}, in both cases the uncertainty in their determination is similar to the possible variation of the parameter along time, so we are not able to conclude that they have changed as a consequence of degradation.

To sum up, the coefficients of temperature of the degraded PV modules have been estimated and from the obtained results it is possible to conclude that, whereas β seems to be stable during the 21 years of exposure, the values of α and γ have experimented important drops. However, when considering the normalized values of these coefficients, the effect of degradation is canceled and the nominal values are still valid.

references

[1] Hoffman AR, Ross RG. Environmental qualification testing of terrestrial solar cell modules. In: 13th IEEE Photovoltaic Specialists Conference PVSC Washington (DC, USA); 1978. p. 835–842. https://ntrs.nasa.gov/search.jsp?R=19790057008, https://www2.jpl.nasa.gov/adv_tech/photovol/ppr_75-80/Envr%20Qual%20Testing%20of%20Terr%20Modules-PVSC1978.pdf.

[2] Köntges M, Kurtz S, Packard C, Jahn U, Berger KA, Kato K, et al. Review of Failures of Photovoltaic Modules. No. IEA-PVPS T13-01:2014, International Energy Agency IEA; 2014. https://iea-pvps.org/key-topics/review-of-failures-of-photovoltaic-modules-final/.

[3] Pozza A, Sample T. Crystalline silicon PV module degradation after 20 years of field exposure studied by electrical tests, electroluminescence, and LBIC. Progress in Photovoltaics: Research and Applications 2016;24(3):368–378. https://doi.org/10.1002/pip.2717.

[4] Cereghetti N, Bura E, Chianese D, Friesen G, Realini A, Rezzonico S. Power and energy production of PV modules statistical considerations of 10 years activity. In: 3rd IEEE World Conference on Photovoltaic Energy Conversion WCPEC, vol. 2 Osake (Japan); 2003. p. 1919–1922. http://ieeexplore.ieee.org/document/1306315.

[5] Osterwald CR, Adelstein J, del Cueto JA, Kroposki B, Trudell D, Moriarty T. Comparison of Degradation Rates of Individual Modules Held at Maximum Power. In: 4th IEEE World Conference on Photovoltaic Energy Conversion WCPEC, vol. 2 Waikoloa (HI, USA); 2006. p. 2085–2088. https://doi.org/10.1109/WCPEC.2006.279914.

[6] Sánchez–Friera P, Piliougine M, Peláez J, Carretero J, Sidrach–de–Cardona M. Analysis of degradation mechanisms of crystalline silicon PV modules after 12 years of operation in Southern Europe. Progress in Photovoltaics: Research and Applications 2011;19(6):658–666. https://doi.org/10.1002/pip.1083.

[7] Ishii T, Takashima T, Otani K. Long-term performance degradation of various kinds of photovoltaic modules under moderate climatic conditions. Progress in Photovoltaics: Research and Applications 2011;19(2):170–179. https://doi.org/10.1002/pip.1005.

[8] Charrouf O, Betka A, hadef H, Djebabra M, Tiar M. Degradation evaluation of PV modules operating under Northern Saharan environment in Algeria. AIP Conference Proceedings 2017;1814(1):020030. https://doi.org/10.1063/1.4976249.

[9] Lorenzo E, Zilles R, Moretón R, Gómez T, Martínez de Olcoz A. Performance analysis of a 7–kW crystalline silicon generator after 17 years of operation in Madrid. Progress in Photovoltaics: Research and Applications 2014;22(12):1273–1279. https://doi.org10.1002/pip.2379.

[10] Chattopadhyay S, Dubey R, Kuthanazhi V, John JJ, Solanki CS, Kottantharayil A, et al. Visual Degradation in Field-Aged Crystalline Silicon PV Modules in India and Correlation With Electrical Degradation. IEEE Journal of Photovoltaics 2014 Nov;4(6):1470–1476. https://doi.org/10.1109/JPHOTOV.2014.2356717.

[11] Kaplani E. Degradation in field–aged crystalline silicon photovoltaic modules and diagnosis using electroluminescence imaging. In: 8th International Workshop on Teaching in Photovoltaics IWTPV Prague (Czech Republic); 2016. https://ueaeprints.uea.ac.uk/id/eprint/58215/.

[12] Características Módulo Fotovoltaico I–53. 7 ed. Málaga (Spain): Isofotón S.A.; 2003. https://www.dropbox.com/s/719xnjopgm46ujp/i53.pdf.

[13] AEMET. OpenData Application Programming Interface. Agencia Estatal de Meteorología. Gobierno de España; (last access 2020/07/30). https://opendata.aemet.es/centrodedescargas/inicio.

[14] Piliougine M, Carretero J, Mora-López L, Sidrach-de-Cardona M. Experimental system for current–voltage curve measurement of photovoltaic modules under outdoor conditions. Progress in Photovoltaics: Research and Applications 2011;19(5):591–602. http://dx.doi.org/10.1002/pip.1073.

[15] Piliougine M, Carretero J, Mora-López L, Sidrach-de-Cardona M. New software tool to characterize photovoltaic modules from commercial equipment. WEENTECH Proceedings in Energy 2018;p. 211–220. https://doi.org/10.32438/WPE.6218.

[16] Fluke 8842A Digital Multimeter – Instruction Manual. 3 7/96 ed. Everett (WA, USA): Fluke Corporation; 1999. https://www.dropbox.com/s/uem2ukva19un1f0/FLUKE8842A.pdf?dl=0.

[17] Agilent 34410A/11A Multimeter User's Guide. 5 ed. Santa Clara (CA, USA): Agilent Technologies; 2012. https://www.dropbox.com/s/wsvrsam9sd1av7r/Agilent34411A.pdf?dl=0.

[18] Precision Pyranometer CM21 – Instruction Manual. 0304 ed. Delft (Holland): Kipp & Zonen; 2004. https://www.dropbox.com/s/hln7wqhoakb2ax6/KIPPZONEN_cm21.pdf?dl=0.

[19] Pyranometer MS-80 – Instruction Manual. 3 ed. Tokyo (Japan): EKO Instruments Co Ltd; 2019. https://www.dropbox.com/s/zumf6389m6vttdj/EKO_MS80V3.pdf?dl=0.

[20] Fluke 2620A/2625A Hydra Series II Data Acquisition Unit, Hydra Series II Data Logger – Users Manual. Everett (WA, USA): Fluke Corporation; 1997. https://www.dropbox.com/s/8tp344xhpt9dsrs/FLUKE_HYDRA.pdf?dl=0.

[21] Compact FieldPoint cFP-21xx and cFP-BP-x – User Manual. Austin (TX, USA): National Instruments; 2005. https://www.dropbox.com/s/7gxfnw8zll1ksun/cFP_2120.pdf?dl=0.

[22] Emery K. Photovoltaic calibrations at the National Renewable Energy Laboratory and uncertainty analysis following the ISO 17025 guidelines. No. NREL/TP-5J00-66873, Golden (CO, USA): National Renewable Energy Laboratory NREL; 2016. https://www.nrel.gov/docs/fy17osti/66873.pdf.

[23] Salam Z, Ishaque K, Taheri H. An improved two–diode photovoltaic (PV) model for PV system. In: Joint International Conference on Power Electronics, Drives and Energy Systems India; 2010. p. 1–5. https://doi.org/10.1109/PEDES.2010.5712374.

[24] Matlab Optimization Toolbox. User's guide. R2020a. Natick (MA, USA): MathWorks; 2020. https://it.mathworks.com/help/pdf_doc/optim/optim.pdf.

[25] IEC 60891. Photovoltaic devices – Procedures for temperature and irradiance corrections to measured *I–V* characteristics. 2 ed. Geneva (Switzerland): International Electrotechnical Commission IEC; 2009. https://webstore.iec.ch/publication/3821.

[26] King DL, Kratochvil JA, Boyson WE. Temperature coefficients for PV modules and arrays: measurement methods, difficulties, and results. In: 26th IEEE Photovoltaic Specialists Conference PVSC Anaheim (CA, USA); 1997. p. 1183–1186. https://doi.org/10.1109/PVSC.1997.654300.

[27] Ding J, Cheng X, Fu T. Analysis of series resistance and *P-T* characteristics of the solar cell. Vacuum 2005;77(2):163 – 167. https://doi.org/10.1016/j.vacuum.2004.08.019.

[28] ISO/IEC Guide 98-3. Uncertainty of measurement – Part 3: Guide to the expression of uncertainty in measurement (GUM:1995). 1 ed. Geneva (Switzerland): International Organization for Standardization ISO; 2008. https://www.iso.org/standard/50461.html.

[29] Whitfield K, Osterwald CR. Procedure for determining the uncertainty of photovoltaic module outdoor electrical performance. Progress in Photovoltaics: Research and Applications 2001;9(2):87–102. https://doi.org/10.1002/pip.356.

[30] Lichten W. Data and Error Analysis. 2 ed. Upper Saddle River (NJ, USA): Prentice Hall; 1999. https://www.pearson.com/us/higher-education/program/Lichten-Data-and-Error-Analysis-2nd-Edition/PGM128560.html.

[31] Kratzenberg MG, Beyer HG, Colle S, Albertazzi A. Uncertainty Calculations in Pyranometer Measurements and Application. In: ASME 2006 International Solar Energy Conference Denver (CO, USA); 2006. p. 689–698. https://doi.org/10.1115/ISEC2006-99168.

[32] Nakos JT. Uncertainty analysis of thermocouple measurements used in normal and abnormal thermal environment experiments at Sandia's Radiant Heat Facility and Lurance Canyon Burn Site. No. SAND2004-1023, Albuquerque (NM, USA): Sandia National Laboratories; 2004. https://doi.org/10.2172/918777.

[33] IEC 60751. Industrial platinum resistance thermometers and platinum temperature sensors. 2 ed. Geneva (Switzerland): International Electrotechnical Commission IEC; 2008. https://webstore.iec.ch/publication/3400.

[34] Dirnberger D, Bartke J, Steinhüser A, Kiefer K, Neuberger F. Uncertainty of Field *I–V* Curve Measurements in Large Scale PV Systems. In: 25th European Photovoltaic Solar Energy Conference and Exhibition EU PVSEC / 5th World Conference on Photovoltaic Energy Conversion WCPEC; 2010. p. 4587 – 4594. https://doi.org/10.4229/25thEUPVSEC2010-4BV.1.62.

[35] Packard CE, Wohlgemuth JH, Kurtz SR. Development of a Visual Inspection Data Collection Tool for Evaluation of Fielded PV Module Condition. No. NREL/TP-5200-56154, Golden (CO,USA): National Renewable Energy Laboratory NREL; 2012. https://doi.org/10.2172/1050110.

[36] Skoczek A, Sample T, Dunlop ED. The results of performance measurements of field-aged crystalline silicon photovoltaic modules. Progress in Photovoltaics: Research and Applications 2009;17(4):227–240. https://doi.org/10.1002/pip.874.

[37] López–García J, Pozza A, Sample T. Long–term soiling of silicon PV modules in a moderate subtropical climate. Solar Energy 2016;130:174 – 183. https://doi.org/10.1016/j.solener.2016.02.025.

[38] Chang M, Chienyu Chen, Hsueh CH, Hsieh WJ, Yen E, Ho KL, et al. The reliability investigation of PV junction box based on 1GW worldwide field database. In: 42nd IEEE Photovoltaic Specialists Conference PVSC New Orleans (LA, USA); 2015. p. 1–4. https://doi.org/10.1109/PVSC.2015.7356130.

[39] Sastry OS, Saurabh S, Shil SK, Pant PC, Kumar R, Kumar A, et al. Performance analysis of field exposed single crystalline silicon modules. Solar Energy Materials and Solar Cells 2010;94(9):1463 – 1468. https://doi.org/10.1016/j.solmat.2010.03.035.

[40] Newmiller J. DNV GL White Paper on Photovoltaic Module Degradation. No. RANA-WP-03-A, San Ramon (CA, USA): DNV KEMA Renewables, Inc.; 2015. https://www.dnvgl.com/publications/photovoltaic-module-degradation-165278.

[41] Quintana MA, King DL, McMahon TJ, Osterwald CR. Commonly observed degradation in field-aged photovoltaic modules. In: 29th IEEE Photovoltaic Specialists Conference PVSC New Orleans (LA, USA); 2002. p. 1436–1439. https://doi.org/10.1109/PVSC.2002.1190879.

[42] Ndiaye A, Charki A, Kobi A, Kébé CMF, Ndiaye PA, Sambou V. Degradations of silicon photovoltaic modules: A literature review. Solar Energy 2013;96:140 – 151. https://doi.org/10.1016/j.solener.2013.07.005.

[43] Kaplanis S, Kaplani E. Energy performance and degradation over 20 years performance of BP c—Si PV modules. Simulation Modelling Practice and Theory 2011;19(4):1201 – 1211. https://doi.org/10.1016/j.simpat.2010.07.009.

[44] Dhimish M, Holmes V, Mehrdadi B, Dales M. The impact of cracks on photovoltaic power performance. Journal of Science: Advanced Materials and Devices 2017;2(2):199 – 209. https://doi.org/10.1016/j.jsamd.2017.05.005.

[45] Chamberlin CE, Rocheleau MA, Marshall MW, Reis AM, Coleman NT, Lehman PA. Comparison of PV module performance before and after 11 and 20 years of field exposure. In: 37th IEEE Photovoltaic Specialists Conference PVSC Seattle (WA, USA); 2011. p. 000101–000105. https://doi.org/10.1109/PVSC.2011.6185854.

[46] Jordan DC, Kurtz SR, VanSant K, Newmiller J. Compendium of photovoltaic degradation rates. Progress in Photovoltaics: Research and Applications 2016;24(7):978–989. https://doi.org/10.1002/pip.2744.

[47] Doumane R, Balistrou M, Logerais PO, Riou O, Durastanti JF, Charki A. A Circuit-Based Approach to Simulate the Characteristics of a Silicon Photovoltaic Module With Aging. Journal of Solar Energy Engineering 2015 04;137(2):021020. https://doi.org/10.1115/1.4029541.

[48] Bouaichi A, Merrouni AA, Hajjaj C, Zitouni H, Ghennioui A, Amrani AE, et al. In–situ inspection and measurement of degradation mechanisms for crystalline and thin film PV systems under harsh climatic conditions. Energy Procedia 2019;157:1210 – 1219. https://doi.org/10.1016/j.egypro.2018.11.287.

[49] Quansah DA, Adaramola MS, Takyi G, Edwin IA. Reliability and Degradation of Solar PV Modules – Case Study of 19—year—old Polycrystalline Modules in Ghana. Technologies 2017;5(2). https://doi.org/10.3390/technologies5020022.

[50] Reis AM, Coleman NT, Marshall MW, Lehman PA, Chamberlin CE. Comparison of PV module performance before and after 11–years of field exposure. In: 29th IEEE Photovoltaic Specialists Conference PVSC New Orleans (LA, USA); 2002. p. 1432–1435. https://doi.org/10.1109/PVSC.2002.1190878.

[51] Bastidas-Rodríguez JD, Franco E, Petrone G, Ramos-Paja CA, Spagnuolo G. Model–Based Degradation Analysis of Photovoltaic Modules Through Series Resistance Estimation. IEEE Transactions on Industrial Electronics 2015 11;62(11):7256–7265. https://doi.org/10.1109/TIE.2015.2459380.

[52] Nehme B. Increase of photovoltaic panels lifespan by monitoring and control. No. HAL Id: tel-02499041, Marseille (France).; 2016. https://hal.archives-ouvertes.fr/tel-02499041.

[53] Emery K, Burdick J, Caiyem Y, Dunlavy D, Field H, Kroposki B, et al. Temperature dependence of photovoltaic cells, modules and systems. In: 25th IEEE Photovoltaic Specialists Conference PVSC Washington (DC, USA); 1996. p. 1275–1278. https://doi.org/10.1109/PVSC.1996.564365.

[54] Mitterhofer S, Glažar B, Jankovec M, Topič M. The Development of Thermal Coefficients of Photovoltaic Devices. Journal of Microelectronics, Electronic Components and Materials 2019;49(4):219 – 227. https://doi.org/10.33180/InfMIDEM2019.404.

[55] Berthod C, Strandberg R, Odden JO, Sætre TO. Reduction of temperature coefficients in multicrystalline silicon solar cells after light–induced degradation. In: 42nd IEEE Photovoltaic Specialists Conference PVSC New Orleans (LA, USA); 2015. p. 1–5. https://doi.org/10.1109/PVSC.2015.7355753.